Partial to full composite action in steel–concrete sandwich beams: development of a modeling strategy and comparison to standards

Robine Calixte, Ludovic Jason, Luc Davenne

Partial to full composite action in steel concrete sandwich beams. Development of a modelling strategy and comparison to standards

Authors: R. Calixte[a,b], L. Jason[a], L. Davenne[b]

[a] Université Paris-Saclay, CEA, Service d'Études Mécaniques et Thermiques, 91191, Gif-sur-Yvette, France
e-mail : ludovic.jason@cea.fr

[b]LEME, UPL, Université Paris Nanterre,
92410 Ville d'Avray, France
e-mail : luc.davenne@parisnanterre.fr

Abstract: In modular steel – concrete – steel (SCS) structures, a partial composite action may appear in some unfavorable conditions, requiring the modeling tools to be adapted to both full and partial composite actions. This study thus proposes a refined simulation methodology, including regularization techniques in tension and compression, to assess full and partial composite actions in SCS structures using 3D finite elements. It is validated on two three-point bending beams. A good agreement on global (resistance) and local (failure mode) experimental quantities is obtained. The modelling strategy is then used to discuss the transition point between the full and the partial composite actions in terms of stud spacing. This numerical analysis is finally compared to existing standards requirements, which shows a good agreement between standards and confirms their conservative tendencies in most situations.

Keys words: Steel-concrete-steel sandwich beams, numerical strategy, full composite action, partial composite action, interfacial slip

Partial to full composite action in steel concrete sandwich beams. Development of a modelling strategy and comparison to standards

Abstract: In modular steel – concrete – steel (SCS) structures, a partial composite action may appear in some unfavorable conditions, requiring the modeling tools to be adapted to both full and partial composite actions. This study thus proposes a refined simulation methodology, including regularization techniques in tension and compression, to assess full and partial composite actions in SCS structures using 3D finite elements. It is validated on two three-point bending beams. A good agreement on global (resistance) and local (failure mode) experimental quantities is obtained. The modelling strategy is then used to discuss the transition point between the full and the partial composite actions in terms of stud spacing. This numerical analysis is finally compared to existing standards requirements, which shows a good agreement between standards and confirms their conservative tendencies in most situations.

Keys words: Steel-concrete-steel sandwich beams, numerical strategy, full composite action, partial composite action, interfacial slip

---

1. INTRODUCTION

To improve the efficiency in building construction, new structural materials have recently appeared. Among them, steel-concrete-steel sandwich structures (SCS) were introduced in [1] – [3] among others. These composite structures are composed of a concrete core between two steel plates (Figure 1). They were initially designed as an alternative solution for the building of submerged tubular tunnels in the mid-1980s ([4] -[5]). They have then been gradually used in bridge decks (Figure 2 (a), [6]), for the construction of shear walls in high buildings [7], for submerged tunnels [8], [9] or for blast and impact shield walls or liquid and gas containers ([9] and [11]). In the nuclear field, SCS structures have been chosen for the containment internal structures of third generation nuclear power plants (AP1000 [12] (Figure 2 (b)) and US-APWR [13] for example). They are also under consideration for Small Modular Reactors (SMR) or Advanced Light Water Reactors (ALWR) [3].

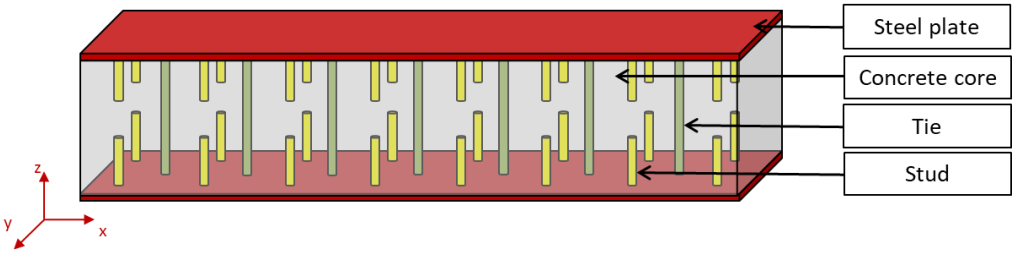

Figure 1 Principle of a SCS beam with studs and ties

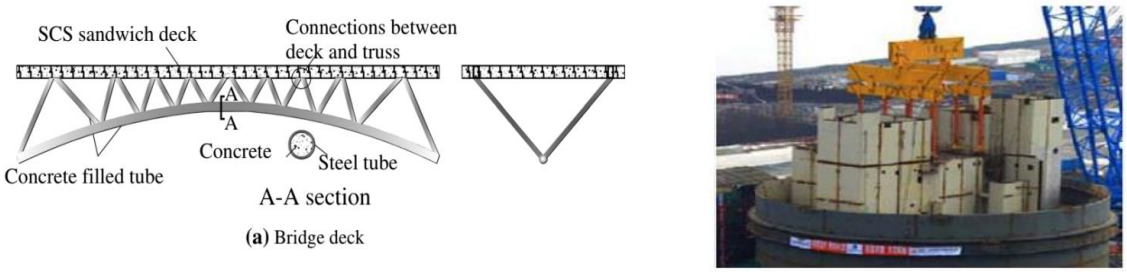

(a) (b)

Figure 2 (a) Example of a SCS sandwich bridge deck [6][5]; (b) AP1000 containment module [14]

In these structures, the main role of the structural concrete is the same as for standard reinforced concrete: it ensures the stiffness and resists compressive stresses. The steel plates is beneficial for tension loading (as reinforcements in reinforced concrete) and their position at the outer fiber of the section increases the moment arm compared to standard reinforced concrete. In [6], [15] and [15], the quality of these structures was highlighted in terms of stiffness, sustainability and strength against extreme loadings. Moreover, SCS structures allow prefabrication of steel units which are also used as lost formwork during concrete pouring. Consequently, in [17], a reduction of the in-site schedule was underlined with a gain of about 30% on the concrete pouring and of about 4% on the complete schedule of the construction work.

The key point to guarantee the efficiency of SCS structures is the overall behavior of the concrete core and the steel plates. The composite action is here ensured by a connection system between both materials. The connection creates a bond between the plate and the core while allowing an interfacial slip to limit the stress concentration. Design methods were proposed in [11], [18] and [19] for the

connection system in order to support the shear forces due to the relative displacement between concrete and steel plates. This connection is generally provided by steel connectors like heads shear stud [20], bi-steel connectors [21] or J-Hook system [22] among others. The quantity of connectors directly defines the nature of the bond. It results in a minimum number of connectors n_{stud}, which can be calculated as:

$$V_l \leq n_{stud} P_{Rd} \quad (1)$$

where, V_l is the horizontal shear force transferred between the concrete core and a steel plate and P_{Rd} is the shear transfer capacity of each connector. Design standards and guides applied to SCS structures or anchorage systems (AISC N690-12s1 [23], Japanese design codes [24], [25], EC4 [26], British standards [27] or ACI 318-08 [28], PCI 6 [29] and Model Code 58 [30]) classically use this equation for the design of the shear connection.

When the number of connectors is sufficient, the full composite action is obtained. The behavior of a SCS beam is then similar to the one of a reinforced concrete beam. In this case, the bond between concrete and steel is important enough to ignore the interfacial slip and maintain the connection in an elastic phase ([10], [31], [32]). The steel plates work like passive reinforcement and the strength of the beam depends only on the concrete and steel loading capacities respectively in compression and in tension. A shear failure appears, with a 45° inclined crack between the lower fiber and the loading point. A buckling of the steel plates can also be observed (Figure 3 (a) [33]).

(a) (b)

Figure 3 Failure of (a) a full composite action SCS bending beam (b) a partial composite action SCS bending beam [33]

Even if the full composite action is generally required, in some situations, a partial composite action may appear. At least, the transition between a full and a partial composite action needs to be clearly identified. For example, increasing the number of studs can lead to construction and welding difficulties or economic inefficiency ([33]and [34]). The number of connectors has therefore to be reasonably limited. Moreover, poor concrete pouring, concrete cracks or buckling of steel plates [35] may lead to a reduction of the bond between the concrete core and the steel plates, which increases the slip at the interface and changes the nature of the composite action. This resulting partial composite action is generally characterized by a horizontal shear failure ([2] and [36]), which is associated to a significant bond slip at the interface between the concrete core and the steel plates (Figure 3 (b)).

Full composite action on SCS structures has been widely investigated in both experimental ([19], [36], [37], [38] and [20] among others) and numerical studies. For example, in [39], the connection system, the steel plates and the concrete core of a SCS shear wall are modeled using 1D beam, 2D shell and 3D volume elements respectively. Friction is considered between concrete and steel plates while a perfect bond is simulated between concrete and studs and between studs and steel plates. The strength and the initial stiffness of the system are reproduced as well as the shape of the post-peak hysteresis during cyclic loads. In [40], the three main components of SCS structures are modeled with 3D elements, considering hard contact and friction between them. A 0D element is added between the connector and the plates to reproduce the evolution of the slip at the interface. A good agreement is obtained on the concrete damage and the failure mode but differences appear in the post-peak phase on the global quantities.

The studies on the partial composite action in SCS structures are much more limited. In [41], a model is proposed for a beam with a limited number of connectors. The steel plates and the concrete core are modeled using 2D shell and 3D volume elements respectively while the connection system is introduced through a recalibration of concrete parameters. In this simulation, steel and concrete are perfectly bonded. The strength of the beam is reproduced. However, as the connectors are not explicitly modeled, the simulated structural damage is not representative. A finer model is presented in [36]. For this study, similarly to [40], the connectors are modeled with 1D beam elements and are related to the plates through

a punctual bond element which integrates an evolution law for the slip as a function of the shear force applied to the connector. A good agreement is obtained on the global behavior (initial stiffness and strength especially). However, the failure of the system and the crack patterns are less accurate. This brief overview, which can be complemented with additional references ([42], [43], [44] and [45]) illustrates that, in the case of a partial composite action, the significant slip between the concrete and the steel plates creates a local non-linearity, which strongly influences the structural behavior.

This paper aims at investigating the transition point between full and partial composite actions, using a unique modelling strategy. The numerical models is first presented. It is then validated on two SCS experimental three point bending beams. A parametric study is then launched to discuss the transition point between a partial and a full composite action. This quantity is finally compared to the different standards requirements to evaluate its representativeness and the expected conservative nature of the standards.

2. PROPOSITION OF A UNIQUE MODELLING STRATEGY FOR SCS COMPOSITE BENDING BEAMS

In this section, a numerical methodology is proposed to represent both full and partial composite actions in SCS structures. It is applied on two experimental three-point bending beams for validation.

2.1. Reference experimental test cases

The experimental results from [36] are considered. SP1-1 and SP1-2 beams are chosen. They have the same geometry (Figure 4 and Table 1) but include a different number of welded headed shear studs (average stud spacing S of $152\ mm$ and $304\ mm$ in two rows for SP1-1 and SP1-2 beams respectively). The three-point bending beams are simply supported with a load applied at the mid-span. The applied load, the cracking evolution and the vertical displacements at mid-span, at the loading points and at the supports are experimentally monitored. Shear failure is observed for SP1-1 beam with a 45° inclined crack between the loading point and the lower fiber (Figure 5 (a)). These diagonal cracks appear after the propagation of vertical flexural cracks. The failure of SP1-2 beam is associated to a significant slip

at the interface between the steel plates and the concrete core (interfacial shear failure). The beam finally breaks into two pieces due to a middle flexural crack (Figure 5 (b)). It can be concluded that the first beam is representative of a full-composite action while the second beam is rather representative of a partial composite action. That is why they have been chosen to evaluate the capacity of the proposed numerical methodology to simulate the mechanical behavior of SCS structures.

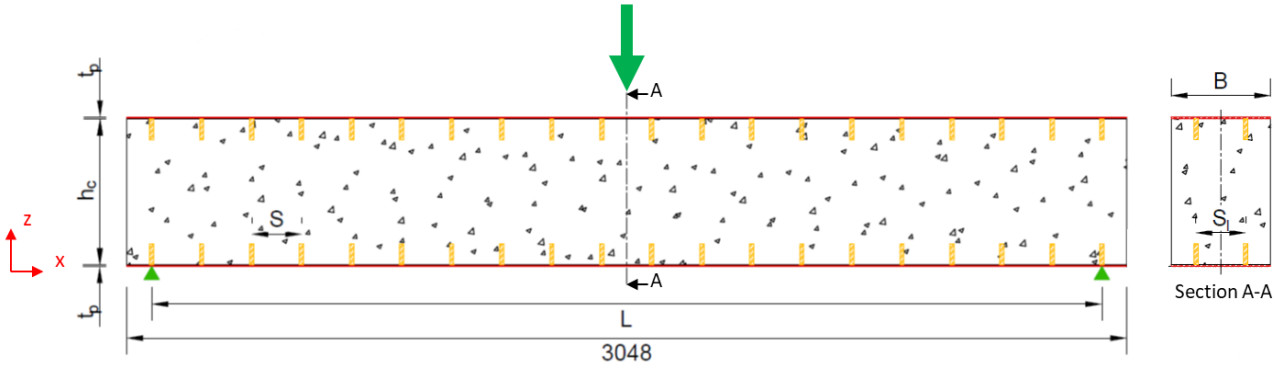

Figure 4 Geometry of the bending beams

Table 1 Geometrical parameters of SP1-1 and SP1-2 beams

Parameters	**Notations**	**SP1-1**	**SP1-2**
Length of beam	$\boldsymbol{L}$ $(\boldsymbol{mm})$	2895.6	
Width of beam	$\boldsymbol{B}$ $(\boldsymbol{mm})$	304.8	
Thickness of steel plate	$\boldsymbol{t_p}$ $(\boldsymbol{mm})$	6.5	
Height of concrete core	$\boldsymbol{h_c}$ $(\boldsymbol{mm})$	445	
Diameter of stud	$\boldsymbol{d_{stud}}$ $(\boldsymbol{mm})$	12.7	
Height of stud	$\boldsymbol{h_{stud}}$ $(\boldsymbol{mm})$	63.5	
Spacing between two studs along the beam width	$\boldsymbol{S_l}$ $(\boldsymbol{mm})$	152.4	
Number of studs per steel plate	$\boldsymbol{n_{stud}}$ $(-)$	40	20
Spacing of the studs along the beam length	$\boldsymbol{S}$ $(\boldsymbol{mm})$	152.4	304.8

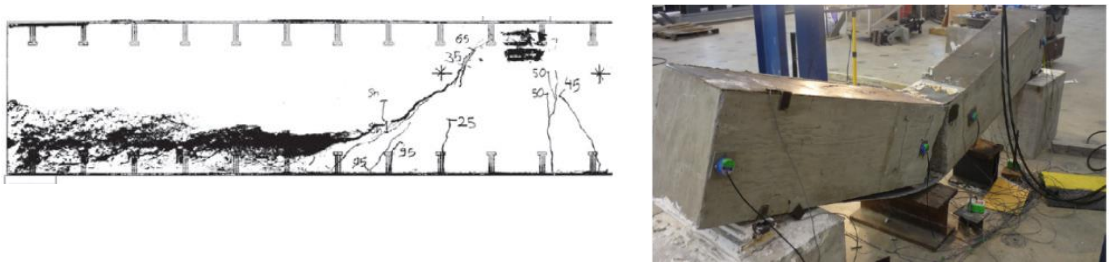

(a) (b)

Figure 5 Failure modes of SP1-1 (a) and SP1-2 (b) beams [20]

2.2. Simulation methodology

A unique numerical methodology is here proposed to represent the mechanical behaviour of the beams. Due to the symmetries of the beam, only one fourth of the structure is modelled. The concrete core, the steel plates and the connectors are represented using 3D solid elements. The size of the finite elements ranges from 1.6 mm (in the section of a connector) to $2d_{stud}$ (in the concrete far from the connectors), where d_{stud} is the diameter of the studs. The total numbers of nodes in the beams are given in Table 2. The meshes are illustrated in Figure 6 (a) – (d).

Table 2 Number of nodes in the numerical models for the bending beams

Number of nodes in	**Concrete core**	**Steel plate**		**One stud**		**Total**
		One plate	**All plates**	**One stud**	**All studs**	
SP1-1	34 436	5 067	10 134	342	6 840	51 410
SP1-2	24 806	3 357	6 714	342	3 420	34 940

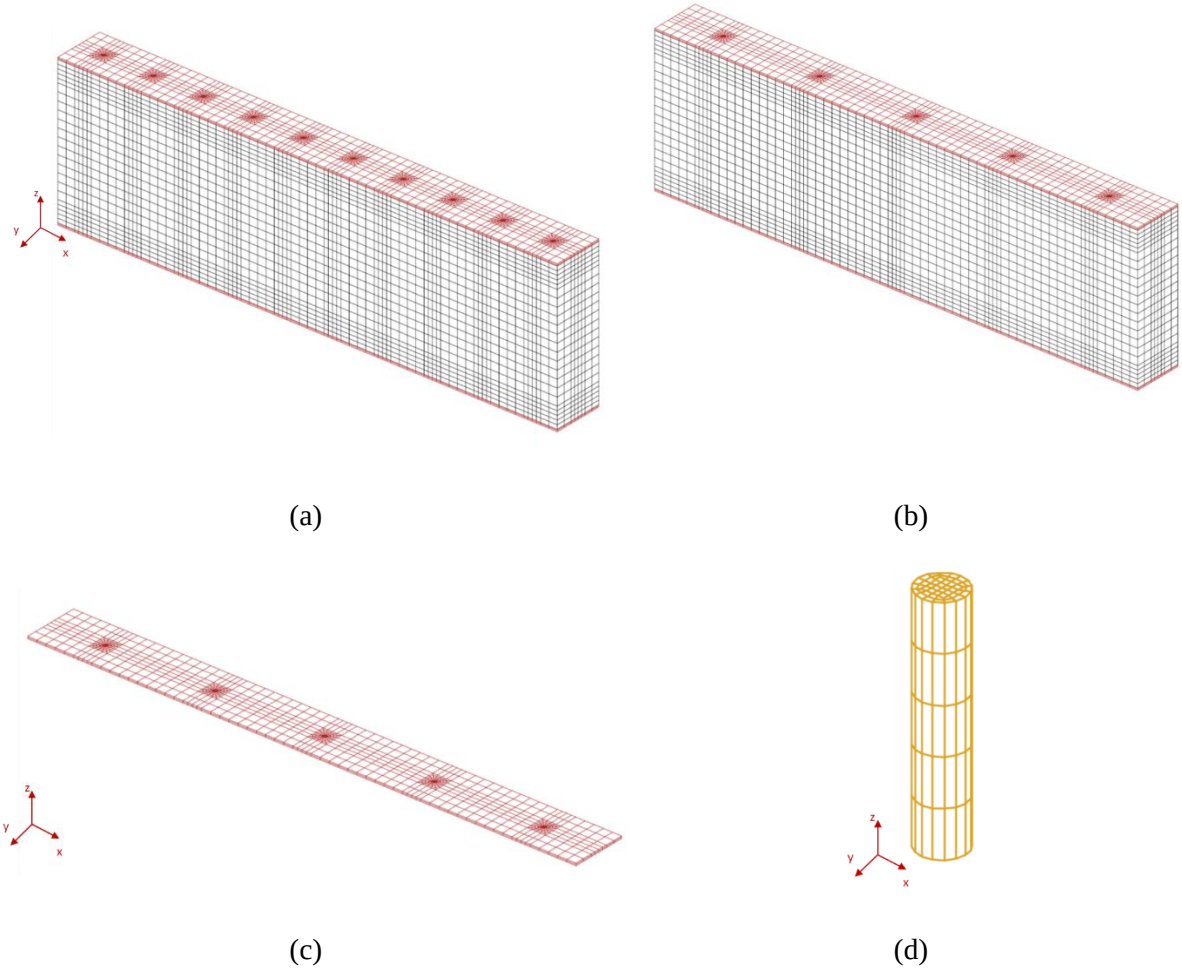

Figure 6 Meshes of SP1-1 (a) and SP1-2 (b) beams; (c) Mesh of one steel plate (SP1-2 beam); (d) Mesh of one stud

Concrete behavior is simulated using an isotropic damage model based on Mazars model in compression [46] and a regularized damage evolution in tension, through a Hillerborg energetic method [47]. This law has been chosen because it allows to correctly reproducing the global behavior in tension and compression with only five model parameters for damage. It introduces a scalar variable D that quantifies the influence of microcracking:

$$\sigma_{ij} = (1 - D)C_{ijkl}\varepsilon_{kl} \quad (2)$$

where σ_{ij} and ε_{kl} are the stress and strain components respectively, C_{ijkl} is the fourth order elastic tensor and D is the damage variable. For the description of the damage growth, an equivalent strain is introduced from the local strain tensor:

$$\varepsilon_{eq} = \sqrt{\sum_{i=1}^{3}(< \varepsilon_i >_+)^2} \quad (3)$$

where $< \varepsilon_i >_+$ are the positive principal strains.

The loading surface g is defined by:

$$g(\varepsilon, D) = \tilde{d}(\varepsilon) - D \quad (4)$$

where the damage variable D is also the history variable which takes the maximum value reached by $\tilde{d}$ during the history of loading

$$D = \max(\tilde{d}, 0) \quad (5)$$

$\tilde{d}$ is defined by an evolution law which distinguishes the mechanical responses of the material in tension and in compression by introducing two scalars D_t and D_c.

$$\begin{aligned}
&\tilde{d}(\varepsilon) = \alpha_t(\varepsilon) D_t(\varepsilon_{eq}) + \alpha_c(\varepsilon) D_c(\varepsilon_{eq}) \\
&D_t = 1 - \frac{\kappa_0}{\varepsilon_{eq}} \exp\left(\frac{l_e . f_{ct}}{G_F}(\kappa_0 - \varepsilon_{eq})\right) \\
&D_c = 1 - \frac{\kappa_0(1 - A_c)}{\varepsilon_{eq}} - \frac{A_c}{\exp[B_c(\varepsilon_{eq} - \kappa_0)]} \\
&\alpha_t = \left(\sum_{i=1}^{3} \frac{< \varepsilon_i^t >< \varepsilon_i >_+}{\varepsilon_{eq}^2}\right)^{\beta} \\
&\alpha_c = 1 - \alpha_t
\end{aligned} \quad (6)$$

D_t and D_c are the tensile and compressive parts of the damage, respectively. The weights α_t and α_c are computed from the strain tensor. They are defined as functions of the principal values of the strains ε_i^t and ε_i^c due to positive and negative stresses respectively. The parameter β reduces the effect of damage under shear compared to tension. l_e is the average size of the finite element (cubic root of the element volume), G_F is the fracture energy and f_{ct} is the tensile strength. κ_0 is a parameter (equal to the ratio between the tensile strength and the Young modulus) and represents the initial threshold from which damage grows. A_c and B_c are two parameters of the model. They are calibrated from uniaxial

compression simulations to obtain the same stress – displacement curve for different values of l_e. The calibration process thus follows the constant compressive cracking energy concept, as defined in [48]. It is one of the originality of the proposed unique modeling strategy, compared to the state-of-the-art. As partial and full composite actions have both to be represented, a particular care has to be taken on the shear and compressive interactions between the concrete core and the steel studs. It is especially the case for partial composite action, for which the interfacial slip may become significant. A compressive "regularization" has thus been added to the classical damage model in order to improve the compressive description of concrete behavior. It is achieved through the proposition of an evolution law for the compressive parameters of the model, as described in Table 4.

The Kuhn – Tucker conditions finally determines the evolution of damage:

$$g \leq 0, \quad \dot{\tilde{d}} \geq 0, \quad g\dot{\tilde{d}} = 0 \tag{7}$$

From the experimental data provided in Table 3, the model parameters are described in Table 4 to obtain the same material properties.

For the steel plates and the steel studs, an elastic plastic behavior with an isotropic hardening is chosen. The parameters, obtained to reproduce the experimental data [36], are given in Table 5.

Table 3 Concrete material properties [36] (values computed from EC2 [49])*

Compressive strength $\boldsymbol{f_c}$ (MPa)	42.06
Tensile strength $\boldsymbol{f_{ct}}$ (MPa)*	3.15
Young modulus $\boldsymbol{E_c}$ (GPa)*	33.85
Poisson's ratio $\boldsymbol{\nu_c}$ (-)	0.2

Table 4 Model parameters for the concrete

$\boldsymbol{A_c}$ (-)	$\boldsymbol{B_c}$ (-)	$\boldsymbol{G_F}$ (J.m^{-2})	$\boldsymbol{\kappa_0}$ (-)	$\boldsymbol{\beta}$ (-)
$67.598l_e^2 + 18.853l_e - 0.0006$	$25713l_e + 1.068$	150	9.31 10^{-5}	1.06

Table 5 Steel materials characteristics

	Plates	**Studs**
Yield limit $\boldsymbol{f_y}$ (MPa)	448.2	488.8
Young modulus $\boldsymbol{E_s}$ (GPa)	201	201
Poisson's ratio $\boldsymbol{\nu_s}$ (-)	0.3	0.3
Tangential modulus $\boldsymbol{E_T}$ (GPa)	0.42	0.42

For the loading and the boundary conditions, the displacement in the vertical direction is blocked along a line at the position of the experimental support (condition a). A vertical displacement is also applied on the upper steel plate at the position of the experimental loading system (condition b). Symmetry conditions are finally considered on both symmetry faces (zero normal displacements for condition c and d) (Figure 7).

A particular attention is also paid to the bond between steel plates, concrete and studs (Figure 8 (a)). A partial bond at the interface between concrete and steel plates is first considered. It assumes a contact that allows a normal separation and a free slip in the tangential directions. If the two surfaces become in contact, equal displacements are then imposed on both materials. The same condition is applied between concrete and studs. A perfect bond, which imposes the same nodal displacements between studs and concrete, is imposed at the end of each stud to represent the effect of the stud heads. Compared to a 3D representation of the head, it may be seen as a simplification of the model. However, it avoids potential meshing difficulties with a significant increase in the number of elements. Finally, the bond between the studs and the plates is obtained through junction elements. These zero dimension finite elements connect each stud node to the associated node of the steel plate through an adapted constitutive law. This law represents the evolution of the bond force as a function of the differential displacements in each direction. In the longitudinal direction of the stud (normal to the cross section), a linear elastic law is supposed. Its stiffness ($K_n = 10^{12} N/m$) is chosen high enough to reproduce the welding of the stud on the plate. In the tangential directions, an elastic plastic law is imposed. The elastic phase corresponds to the welding of the stud ($K_s = 10^{12} N/m$). A plastic limit is then introduced to model the shear failure

of the stud ($P_{Rd} = 49.5\ kN$), which is calculated from [26] with no safety factor (equation 8). An illustration of the constitutive law in one tangential direction is presented in Figure 8 (b).

$$P_{Rd} = 0{,}8 f_{ug} A_{gouj} = 49.5\ kN \tag{8}$$

These particular finite elements for the bond between the studs and the steel plates, and the way they are calibrated (explicitly introducing the shear failure of the stud), represents the second main originality of the proposed numerical strategy. As for the compressive regularization, it is here again especially required when partial composite action wants to be reproduced. In this case, the failure mode is expected to be rather driven by the steel plate – steel studs interaction, which has to be carefully represented.

The simulation is performed using the implicit finite element code Cast3M [50].

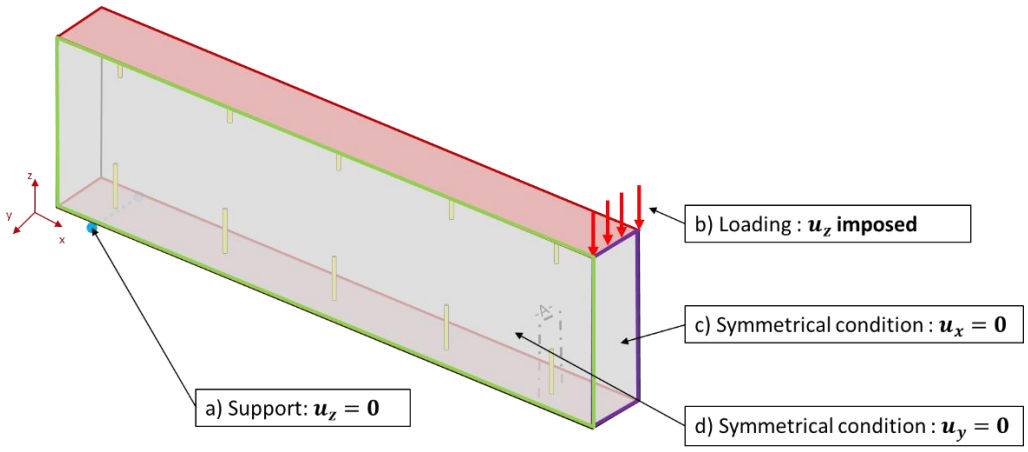

Figure 7 Boundary conditions for the bending beams

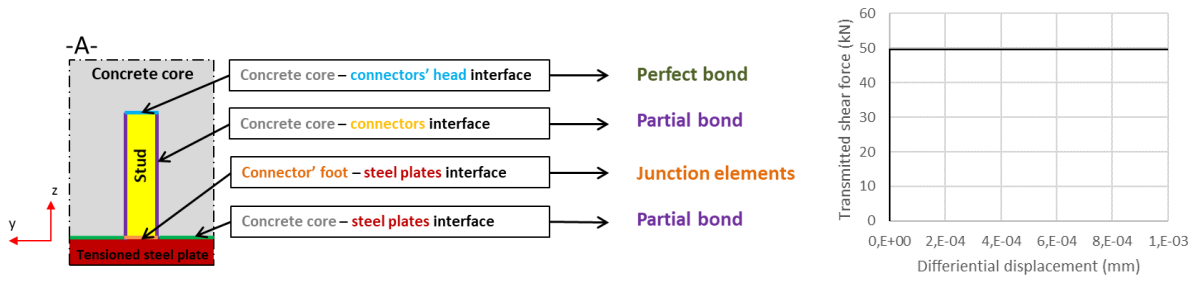

(a) (b)

Figure 8 (a) Interfacial bonds, (b) Constitutive law of the shear stud – steel plate junction interface in a tangential direction

2.3. Results of the reference simulations

Results for SP1 beam are illustrated from Figure 9 to Figure 12. Regarding the global behavior (Figure 9), the overall behavior is correctly reproduced (elastic regime and mechanical degradation). The structural strength is especially obtained, with a difference of about 6% between the experimental and the numerical values. Several partial unloading are observed numerically. The first one corresponds to the initiation of a vertical flexural crack, which modifies the stiffness of the structure. The second unloading can be associated to the opening of a 45° inclined concrete shear crack (258 kN). The following unloading corresponds to the opening of concrete cracks in the lower fiber of the beam. Finally, the overall failure mode is consistent with the experiment (Figure 10 (a)). The experimental and numerical longitudinal strains in the steel plates are also in agreement (Figure 10 (b)). A local yielding of the bottom steel plate is especially obtained numerically near the position of the shear crack. It is to be noted that the increase in the strain in the top steel plate at the midspan is due to the modeling choices and especially to the linear applied load.

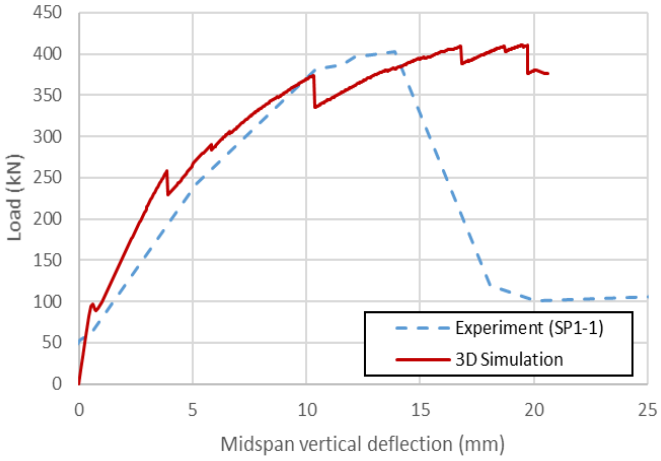

Figure 9 Load – midspan vertical displacement curve of the numerical simulation of the SP1-1 beam

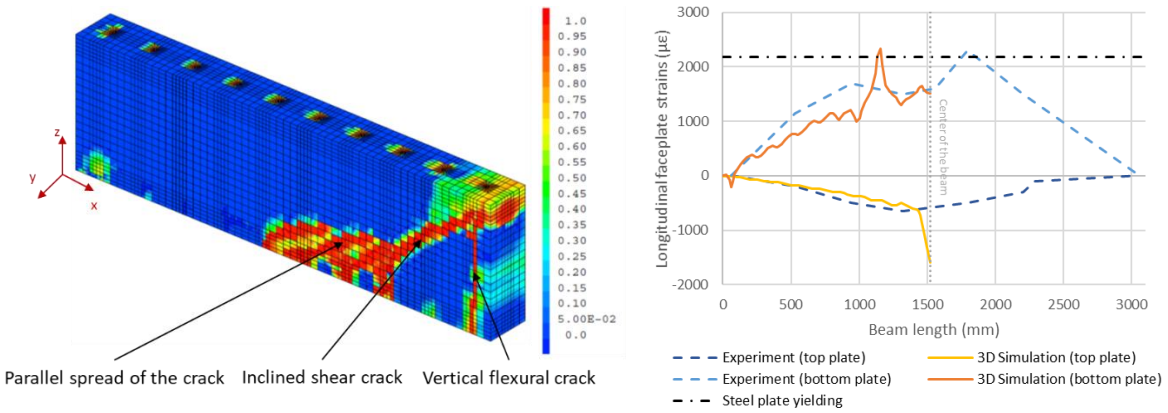

(a) (b)

Figure 10 SP1-1 beam results: (a) final damage distribution in concrete, (b) Longitudinal steel plate strain along the beam for a deflection of 13.9 mm

For SP1-2 beam (expected partial composite action), the global mechanical behavior is also correctly captured (Figure 11) with a lower mechanical resistance, compared to SP1-1 beam. The first unloading corresponds here to the initiation of a vertical flexural crack near the stud, close to the application points of the load. The second unloading (13.9 mm displacement and 256.15 kN load) corresponds to the initiation of a shear crack inclined at more than 45° (Figure 12 (a)). Even if this crack is not observed experimentally, it is to be noted that this failure mode is generally obtained for partial composite action beams ([33] for example). After the peak load, a constant force is observed. It corresponds to the maximum shear force that can be transferred by the junction elements at the interface between the stud and the bottom steel plate. The simulation of the longitudinal strain in the steel plate also shows an overall agreement (Figure 12 (b)). The observed differences may be explained by some model simplifications (no friction between the concrete core and the steel plate, simplification of the studs' heads or simplification of the behavior of the stud – steel plates junction elements with a perfect elastic plastic constitutive law). However, the quantitative and quantitative differences between a full and a partial composite action are clearly underlined with a decrease in the strength of the structure and the change in the failure mode.

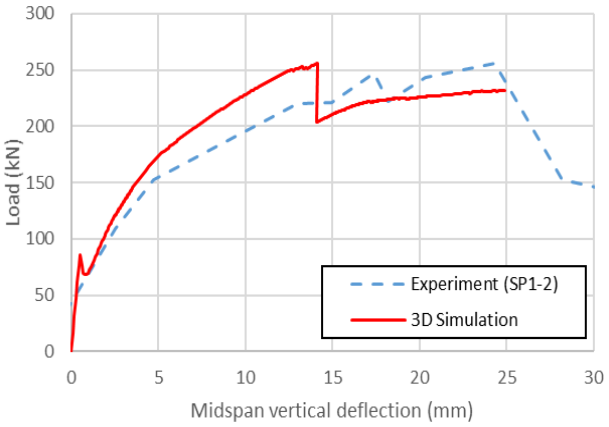

Figure 11 Load – midspan vertical displacement curve of the numerical simulation of the SP1-2 beam

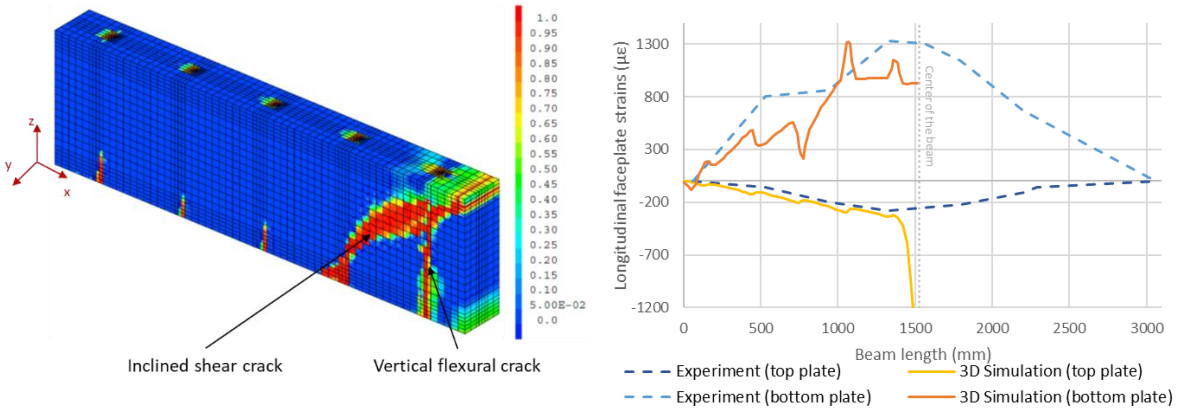

(a) (b)

Figure 12 SP1-2 beam results: (a) final damage distribution in concrete; (b) Longitudinal strain inside the steel plate along the beam for a deflection of 24.3 mm

3. PARTIAL TO FULL COMPOSITE ACTION: NUMERICAL ANALYSIS

Based on the previous results, a parametric study is launched to evaluate the transition point between a partial and a full composite action in the beam. The number of studs in the bending beam is gradually increased (decrease in the stud spacing) from the number of studs in SP1-2 beam ($S = 304.8\,mm$) to 48 studs per steel plate ($S = 127\,mm$) (Table 6). A constant spacing is supposed between each stud. It is to be noted that the mesh needs to be adapted to the number of studs. Examples of meshes are provided in Figure 13.

Table 6. Configurations for the parametric study on the stud spacing

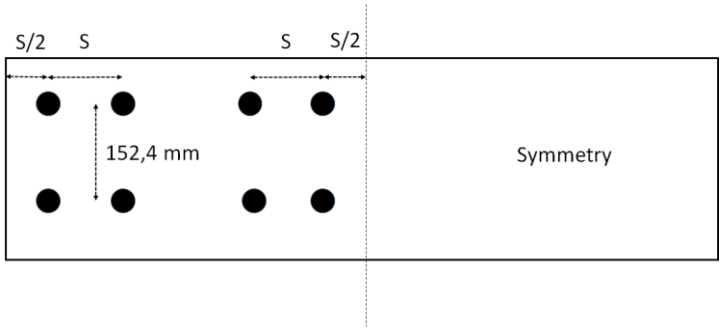

Top view of a steel plate

Stud spacing (mm)	Total number of studs per steel plate
127	48 (24 x 2)
138.5	44 (22 x 2)
152.4 (SP1-1)	40 (20 x 2)
169.3	36 (18 x 2)
190.5	32 (16 x 2)
217.7	28 (14 x 2)
254	24 (12 x 2)
304.8 (SP1-2)	20 (10 x 2)

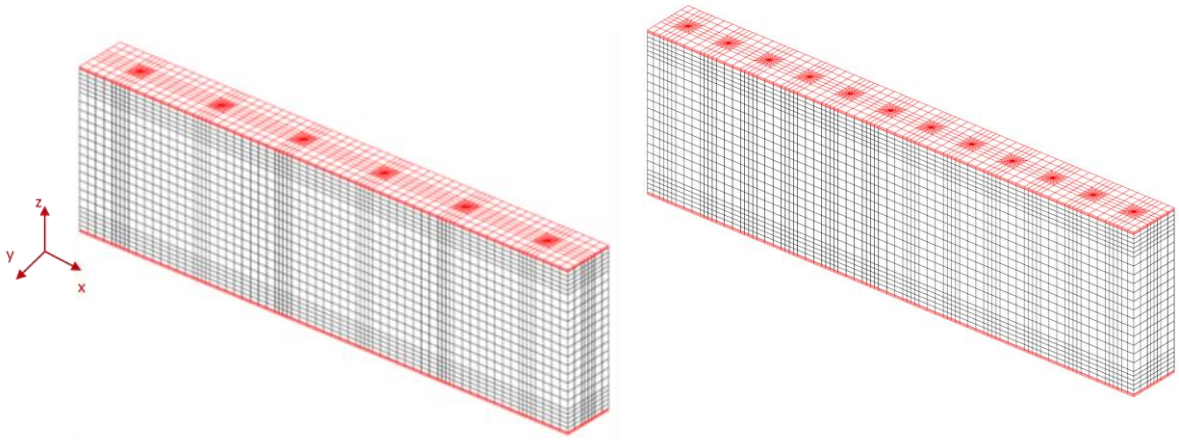

S = 254 mm (24 studs per steel plate)

S = 127mm (48 studs per steel plate)

Figure 13 Examples of the mesh of bending SCS beams (one fourth of the beam)

3.1. Effect of the composite action on the global behavior

Figure 14 and Figure 15 provide midspan vertical displacement as a function of the load for stud spacing between $S = 304.8\,mm$ and $S = 190.5\,mm$ and between $S = 190.5\,mm$ and $S = 127\,mm$, respectively. Similar responses are obtained before the opening of the first flexural concrete crack. Differences can be explained by the different steel ratios due to the stud spacing.

When the flexural crack initiates, changes in the behavior become visible. Two groups of structural responses can then be identified. From $S = 304.8\,mm$ to $S = 190.5\,mm$ (Figure 14), the force – deflection curves show a significant variation as a function of the stud spacing, with, for a given deflection, an increase in the force with decreasing stud spacing. When $S \leq 190.5\,mm$ (Figure 15), the evolution of the curves is less significant, until the initiation of the shear crack (second unloading). These observations give first information about a transition from a partial to a full composition action. However, they may be considered insufficient to identify a precise transition point. That is why the local behaviors are going to be investigated in the next section.

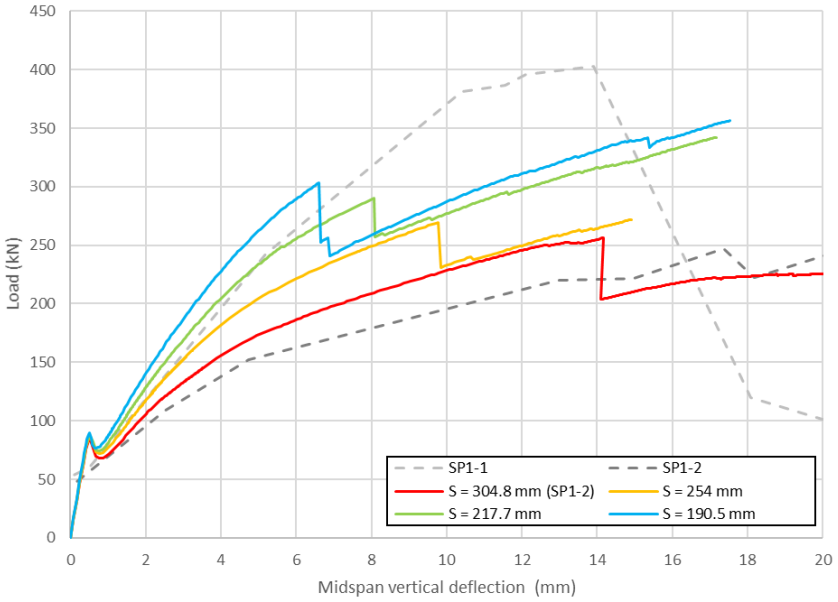

Figure 14 Load – midspan vertical displacement curves for SCS beams with different stud spacings from $S = 304.8\,mm$ to $S = 190.5\,mm$

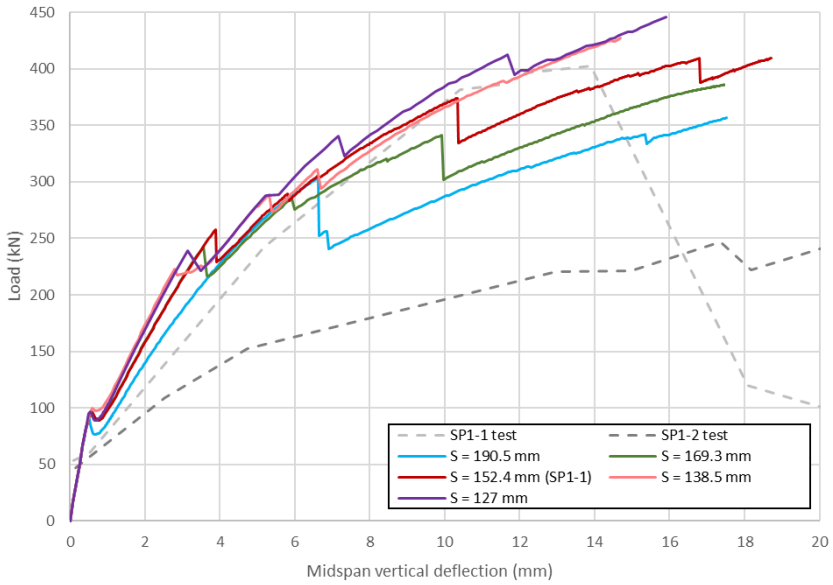

Figure 15 Load – midspan vertical displacement curves for SCS beams with different stud spacings from $S = 190.5\ mm$ *to* $S = 127\ mm$

3.2. Effect of the composite action on the failure mode

Figure 16 (a) provides the longitudinal strain along the bottom steel plate for a deflection of 13.9 mm, which corresponds to the experimental failure in SP1-1 beam (full composite action). For $S < 190.5\ mm$, a yielding of the bottom steel plate is obtained with a longitudinal strain higher than the steel yield strain ($\varepsilon_y = 2186\ \mu\varepsilon$). The local yielding of the bottom steel plate indicates an good contribution of the steel plate and is associated to a full composite action. For $S \geq 190.5\ mm$, no local yielding is observed. In the Figure 16 (b), the longitudinal steel strains do not reach the yield strain and the plate remains in an elastic phase. The failure mode is rather a concrete-driven failure mode, which rather characterizes a partial composite action. A transition criterion between full and partial composite action can thus be defined from this plasticity criterion, for a spacing between $S = 169.3\ mm$ and $S = 190.5\ mm$.

This quantitative analysis is confirmed by the damage distributions (Figure 17). For each beam, at a deflection of 13.9 mm, a vertical localized damage band is observed. For the beams with $S \leq 190.5\ mm$, an inclined crack with a slope lower than 45° can be observed. These shear cracks confirm the failure mode under shear stress, which can be related to a full composite action. A crack, which develops along

the bottom plate, is observed for the beams with $S \leq 169.3\ mm$. In accordance with the experimental results from [19], [20] and [36], this evolution is also related to a full composite action. When $S > 190.5\ mm$, the slope of the inclined crack becomes higher. The failure mode related to a partial composite action is identified. It corresponds to a shear failure with an important interfacial slip, with a lower contribution of the steel plate. These results qualitatively confirm the transition point between the full and the partial composite action for a spacing between S=169.3 mm and S= 190.5 mm.

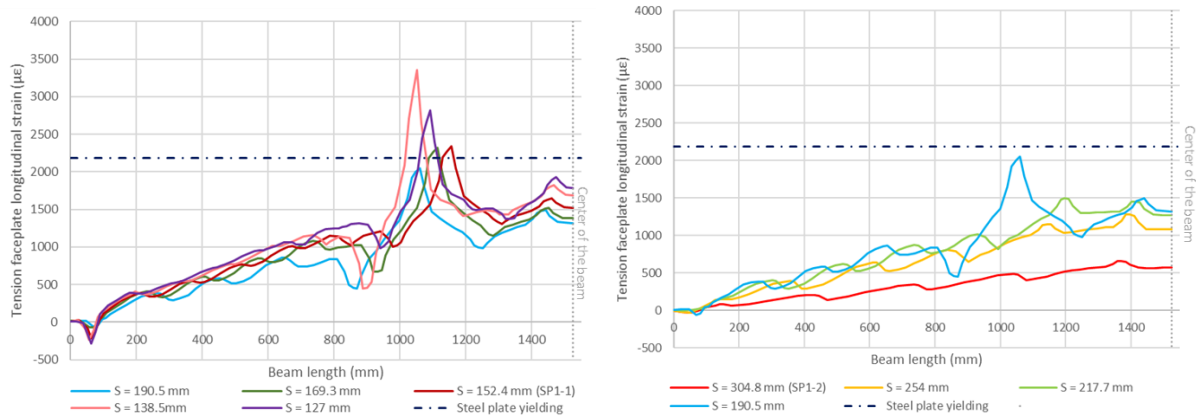

(a) (b)

Figure 16 Longitudinal bottom steel plate strain along the half-beam for a deflection of 13.9 mm for SCS beams with different stud spacing: (a) from $S = 190.5\ mm$ to $S = 127\ mm$; (b) from $S = 304.8\ mm$ to $S = 190.5\ mm$

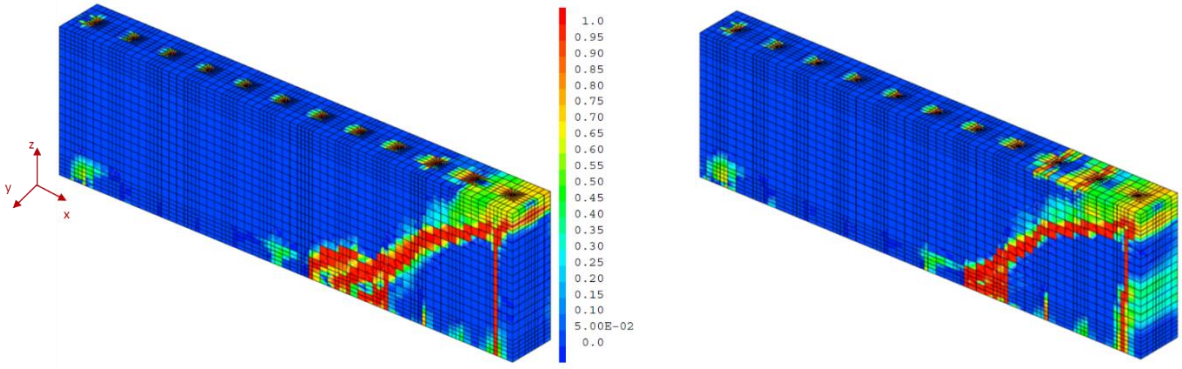

S = 127 mm S = 138.5 mm

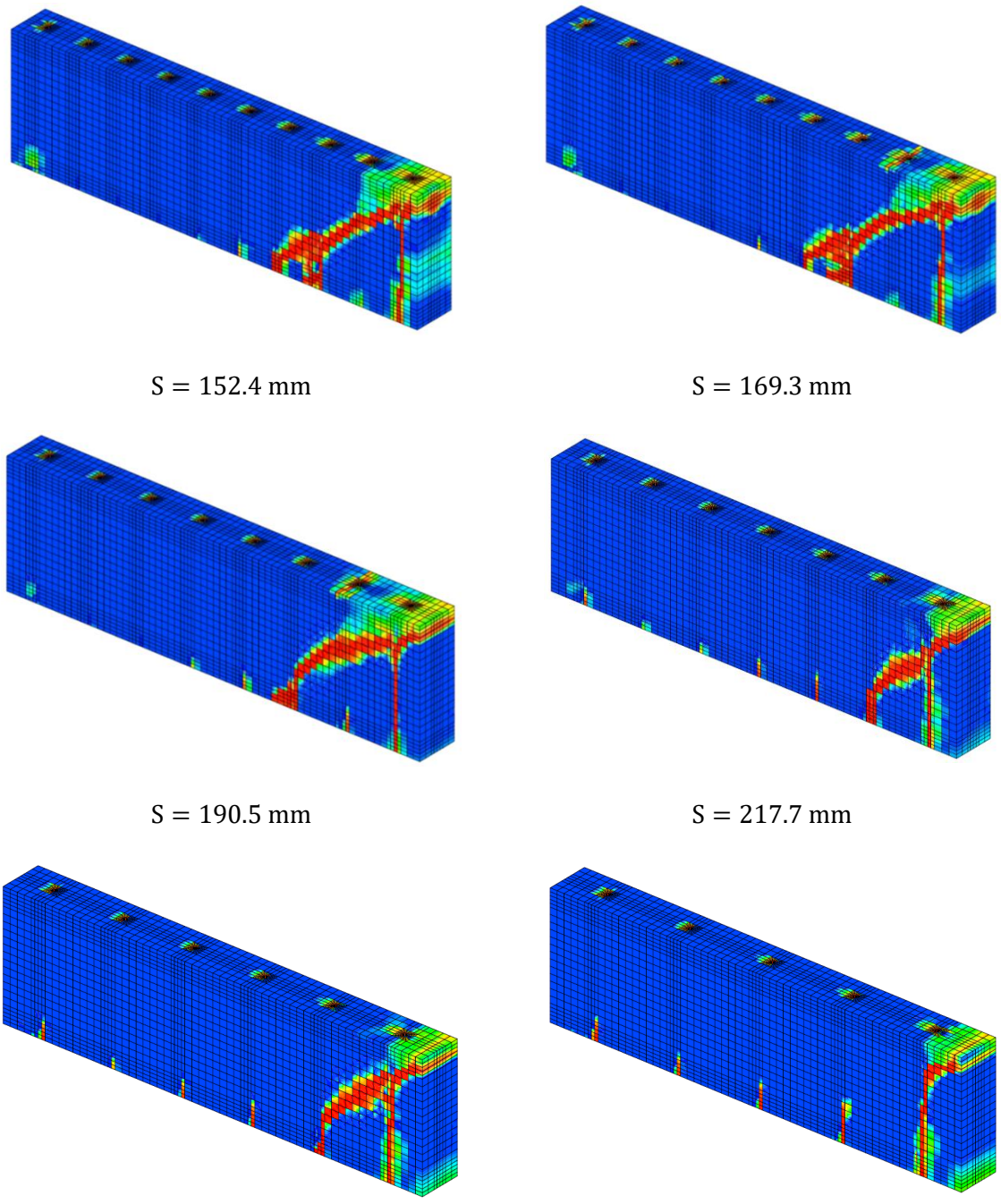

Figure 17 Damage distributions for simulated SCS beams with decreasing studs spacing for a vertical deflection of 13.9 mm

Finally, the interfacial slip is studied. In the state-of-the-art, the partial composite action is indeed related to an increase of the interfacial slip. This interfacial slip directly affects the strength and the stiffness of SCS structures ([9], [25], [31], [50] and [52]).

The distributions of the slip along the center line of the interface between the bottom steel plate and the concrete are given for beams SP1-1 and SP1-2 in Figure 18 (a), for a deflection equal to 0.25 mm (before the first crack initiates). A zero slip is obtained on the symmetry face (x = 1.524 m) due to the applied boundary conditions. Then the bond slip increases along the beam. As expected, the interfacial slip on SP1-2 beam is always higher that on SP1-1 beam, due to a smaller number of connection points. A comparison of the bond slip at the position of the support for a deflection equal to 0.25 mm is presented for different stud spacings in Figure 18 (b). The interfacial bond slip significantly increases with S, when S is more than 169.3 mm, which is in agreement with the transition point discussed in the previous section.

This evolution is modified when cracks appear in concrete and leads to a discontinuity in the interfacial slip. Figure 19 (a) and (b) compare the slip along the bottom interface for beams SP1-1 and SP1-2 after the flexural crack (deflection equal to 2 mm) and at the experimental failure of SP1-1 beam (deflection equal to 13.9 mm). Damage in concrete leads to an important local increase of the slip and redistributions along the structure.

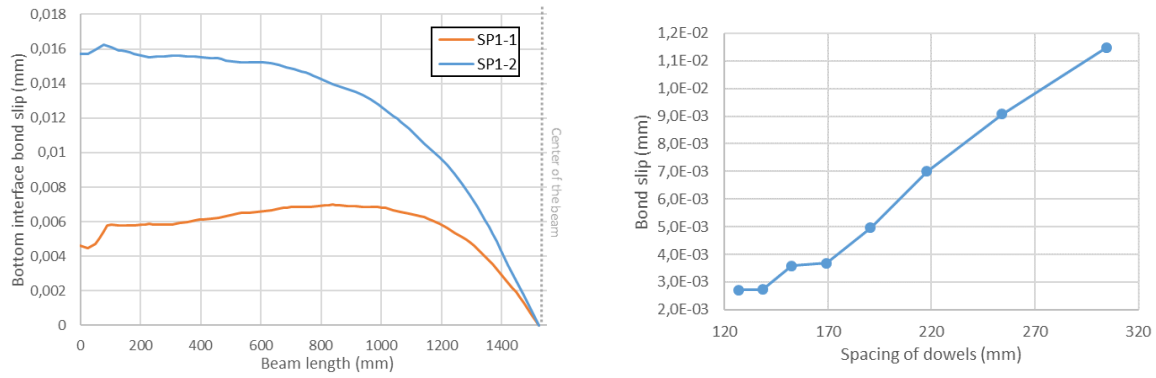

(a) (b)

Figure 18 For a deflection of 0.25mm (a) evolution of the bond slip at the interface between the bottom steel plate and the concrete core for the 3D simulation of SP1-1 and SP1-2 beams; (b) comparison of the bond slip at the lower interface at the left edge of SCS beams for different stud spacing

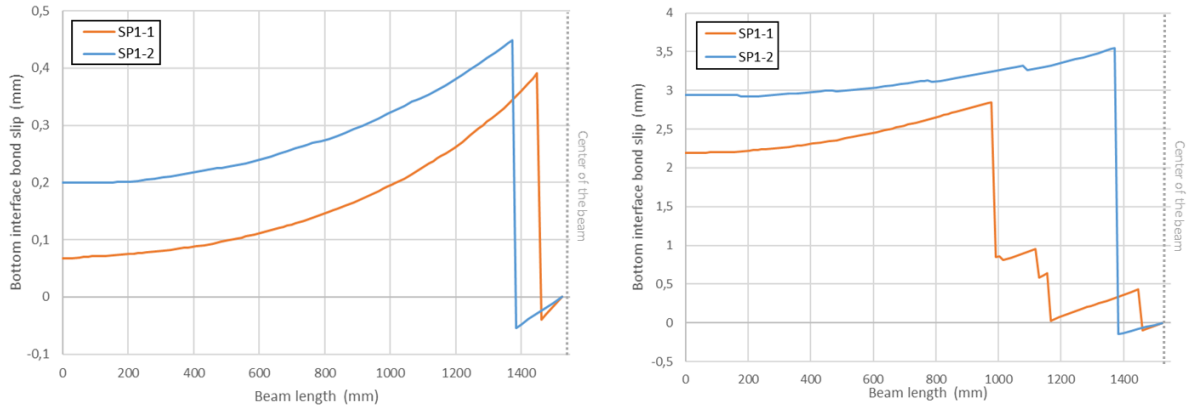

(a) (b)

Figure 19 Evolution of the bond slip at the interface between the bottom steel plate and the concrete core for the 3D simulation of SP1-1 and SP1-2 beams (a) for a deflection of 2mm, (b) for a deflection of 13.9mm

4. DISCUSSION ABOUT STANDARDS FOR FULL COMPOSITE ACTION

In the previous section, it was highlighted how the proposed simulation methodology was able to reproduce both partial and full composite actions. A transition criterion has been discussed from the distribution of the steel strains especially. In this section, the numerical transition between a full and a partial composite action is going to be compared to the standards requirements.

4.1. Standard requirements for the minimum number of studs

Generally, standards specify requirements to achieve a full composite action in composite structures, especially in terms of number of studs. This criterion represents the minimum number of studs n_{stud} to ensure a flexural failure before the shear failure of the studs ([23], [25], [26]). When considering two rows of studs ($S = 2L/n_{stud}$), the following equation gives the criterion on the stud spacing to ensure the full composite action:

$$S \leq \frac{2P_{Rd}L}{V_l} \tag{9}$$

where L is the length of the beam and V_l is the horizontal shear force.

P_{Rd} is the shear transfer capacity of each connector. It is defined from the shear strength of the connector P_{stud} and the concrete pull-out strength P_{conc}:

$$P_{Rd} = \min(P_{stud}; P_{conc}) \quad (10)$$

V_l is obtained considering that the failure of the bending composite beam occurs either by crushing of the concrete ($F_{c,max}$) or by yielding of a steel plate ($F_{s,max}$), depending on their relative dimensions:

$$V_l = \min\left(F_{c,max}; F_{s,max}\right) \quad (11)$$

Table 7 summarizes the different equations provided in EC4 [26], AISC 690 [23], JSCE 15 [24][25], ACI 318-08 [28], PCI 6th [29], BS 5400 [27] and Model code 58 [30]. Differences on the influencing parameters and in the safety coefficients can be observed especially.

Table 7 Comparison of the formulas of the calculation of the minimal number of studs per steel plate to ensure a full composite action from several standards

Standard	**Horizontal interfacial shear stress** $V_l = min(F_{s,max}; F_{c,max})$		**Shear strength of the connection** $P_{Rd} = min(P_{stud}; P_{conc})$	
	$F_{s,max}$	$F_{c,max}$	P_{stud}	P_{conc}
EC4 [26]	$A_{plate}f_y$	$0{,}85A_{core}f_c$	$\frac{0.8A_{stud}f_u}{1.25}$	$\frac{0{,}29\alpha d_{stud}^2\sqrt{f_cE_c}}{1.25}$
AISC 690 [23]	$A_{plate}f_y$	$0{,}85A_{core}f_c$	$0.75\ A_{stud}f_u$	$0.5A_{stud}\sqrt{f_cE_c}$
JSCE 15 [24][25]	$A_{plate}f_y$		$\begin{cases} \frac{9.395d_{stud}^2 f_c^{\frac{1}{2}}}{1.1} & if\ h_{stud}/d_{stud} \geq 5.5 \\ \frac{1.722d_{stud}h_{stud}f_c^{\frac{1}{2}}}{1.1} & if\ h_{stud}/d_{stud} < 5.5 \end{cases}$	
AC1 318-08 [26]	$A_{plate}f_y$	$0{,}85A_{core}f_c$	$0.65\ A_{stud}f_u$	$0.7(24\sqrt{f_c}d_{stud}^{1.5}h_{stud}^{0.5})$
PCI 6th [29]	$A_{plate}f_y$	$0{,}85A_{core}f_c$	$0.75\ A_{stud}f_u$	$0.7(215\sqrt{f_c}d_{stud}^{1.5}h_{stud}^{0.5})$
BS 5400 [27]	$A_{plate}f_y$	$0{,}4A_{core}f_c$	From a table	

Model code 58 [30]	$A_{plate}f_y$	$0{,}85A_{core}f_c$	$\frac{0.6A_{stud}f_u}{1.09}$	$\frac{2}{1.5}(8.9\sqrt{f_c}h_{stud}^{1.5})$

$A_{plate}, A_{core}, A_{stud}$: cross sections of the steel plate, of the concrete core in compression and of a stud; d_{stud}, h_{stud} : diameter and length of the stud; f_y, f_u: yield strength of the steel plate and of the studs, f_c, E_c concrete compressive strength and Young modulus; α is a coefficient to consider the ductility of the stud defined as $\alpha = 0.2\left(\frac{h_{stud}}{d_{stud}} + 1\right)$ if $3 \leq \frac{h_{stud}}{d_{stud}} \leq 4$ and $\alpha = 1$ if $\frac{h_{stud}}{d_{stud}} > 4$

4.2. Comparison between standards and numerical transition

Standards are applied to the bending beams. Results are provided in Table 8. Differences in the maximal stud spacing to ensure a full composite action are observed, from $S = 179.3\,mm$ (JSCE 15) to $S = 117.2\,mm$ (Model code 58)

The calculated numerical transition point is now compared to the standards (Figure 20). It can be observed that the numerical transition point is in a rather good agreement with the standards (same order of magnitude). It thus validates, at least qualitatively, the numerical strategy to define the change from a full to a partial composite action. As expected, the standards remains conservative, as they are based on the overall behavior of the concrete core and the steel plates and considered a zero interfacial slip.

Table 8 Results of the application of standards design of the SP1 beam

	Horizontal interfacial shear stress			**Shear strength of the connection**			$\boldsymbol{S\ (mm)}$	**Failure mode**
Standard	$\boldsymbol{F_{s,max}\ (kN)}$	$\boldsymbol{F_{c,max}\ (kN)}$	$\boldsymbol{V_l\ (kN)}$	$\boldsymbol{P_{stud}\ (kN)}$	$\boldsymbol{P_{conc}\ (kN)}$	$\boldsymbol{P_{Rd}\ (kN)}$		
EC4 [26]	867.5	4849.1	867.5	39.6	44.7	39.6	138.5	Stud shear
AISC 690 [23]	867.5	4849.1		46.4	76.7	46.4	160.4	
JSCE 15 [24][25]	867.5			53.1		53.1	179.3	
AC1 318-08 [28]	867.5	4849.1		40.3	101.7	40.3	138.5	

PCI 6th [29]	867.5	4849.1		46.4	64.4	46.4	160.4	
BS 5400 [27]	867.5	2281.9		37.8		37.8	132.5	
Model code 58 [30]	867.5	4849.1		34.1	39.1	34.1	117.2	

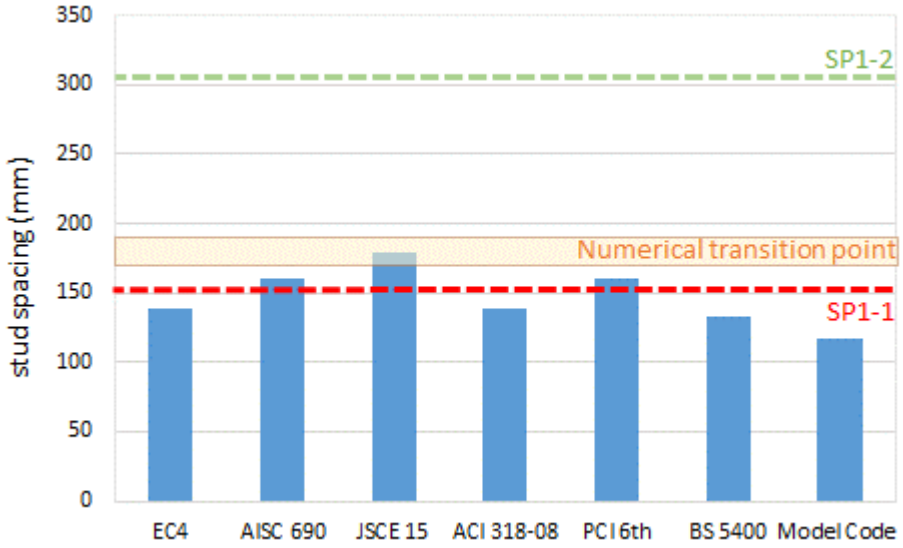

Figure 20 Comparison of the minimal number of studs to ensure the full composite action for standards and the numerical analysis

5. CONCLUSION

Steel-concrete-steel composite structures are sandwich composite structures combining steel plates and a concrete core through a connection system, which ensures the overall behavior. The structure combines the advantages of reinforced concrete and provides a greater resistance under extreme loadings, sustainability and durability. Moreover, the external position of the steel plates allows their use as formwork and leads to a modular structure, which tends to reduce and ease the construction phase. All these advantages make SCS construction a competitive choice in the construction field.

In this contribution, a general simulation methodology was proposed to assess both full and partial composite actions using 3D finite elements, compared to the classical state-of-the art, which generally

considers numerical strategies for either full or partial composite actions. The modeling strategy especially includes two key components, namely a regularization technique in compression and interface elements. It was validated by comparison to experimental results on three point bending beams. The full composite action was associated to a concrete failure in shear and a local yielding of the bottom steel plate while the partial composite action was driven by a horizontal shear failure associated to a significant bond slip at the interfaces between the steel plates and the concrete core.

A transition point between full and partial composite actions was numerically discussed in terms of stud spacing through a numerical parametric study. Using a criterion based on the plastic yielding of the steel plates, a full composite action was obtained for a stud spacing between 169.3 mm and 190.5 mm. The global behavior and the interfacial slip between the concrete core and the steel plates allowed to verify the change of behavior and confirmed this transition point.

The identified numerical criterion was finally compared to the classical standards for composite structures. A good agreement was obtained, considering the expected conservative aspects of the standards. The proposed methodology can thus be seen as an appropriate alternative to the direct application of standards, especially if local quantities need to be studied.

6. ACKNOLEDGMENTS

The authors gratefully acknowledge the partial financial support from EDF R&D for the development and the analysis of the simulation results.

7. REFERENCES

[1] Leekitwattana M, Boyd S.W, Shenoi R.A (2010) An alternative design of steel concrete steel sandwich beam, 9th International Conference on Sandwich Structures (ICSS-9), Pasadena, CA, USA

[2] Leng Y.B., Song X.B. (2016), Experimental study on shear performance of steel-concrete-steel Sandwich Beams, Journal of Constructional Steel Research 38:257-279, https://doi.org/10.1016/j.jcsr.2015.12.017

[3] Varma A.H., Malushte S.R., Lai Z. (2015) Modularity & Innovation using steel-concrete-steel composite (SC) walls for nuclear and commercial construction, 11th International Conference: Advances in Steel-Concrete Composite Structures (ASCCS)

[4] Montague P. (1975) A simple Composite construction for cylindrical shells subjected to external pressure, Journal Mechanical Engineering Science 17(2):105-113, https://doi.org/10.1243/JMES_JOUR_1975_017_016_02

[5] Solomon S.K, Smith D.W, Cursens A.R. (1976), Flexural tests of steel-concrete-steel sandwiches, Magazine of Concrete Research, 28(94):13-20 https://doi.org/10.1680/macr.1976.28.94.13

[6] Yan J.B, Liew J.Y.R, Zhang M.H, Sohel K.M.A (2015), Experimental and analytical study on ultimate strength behavior of steel-concrete-steel sandwich composite beam structures, Materials and Structures, 48:1523-1544, https://doi.org/10.1617/s11527-014-0252-4

[7] AISC (2017), Modern Steel Construction – Steel Core System Revolutionizes High-Rise Construction – AISC https://www.aisc.org/modernsteel/news/

[8] Calatrava, (2013) Sharq Crossing – Santiago Calatrava Architects & Engineers https://calatrava.com/projects/

[9] Bekarlar K (2016) Steel-Concrete-Steel Sandwich Immersed Tunnels For Large Spans, Master thesis dissertation Technische Universiteit Delft

[10] Wright H.D, Oduyemi T.O.S, Evans H.R. (1991) The experimental behavior of double skin composite elements, Journal of Constructional Steel Research 19:97-110, https://doi.org/10.1016/0143-974X(91)90036-Z

[11] Liew J.Y.R, Yan J.B., Huang Z.Y (2016) Steel-concrete-steel sandwich composite structures – recent innovations, Journal of constructional Steel research 130:202-221, https://doi.org/10.1016/j.jcsr.2016.12.007

[12] Westingthouse Electric Company (WEC) (2021) AP1000-PWR, http://www.westingthousenuclear.com/New-Plants/AP1000-PWR

[13] Mitsubishi Heavy Industry (MHI) (2013) Advanced PWR, IAEA INPRO 7th Dialogue Forum,

[14] Lohani V. (2016), Effects of geometric and material parameters on failure modes of SCS elements, Mater thesis dissertation Aalto University School of Engineering

[15] Booth P.N, Varma A.H., Sener K., Malushte S.R (2015) Flexural behavior and design of steel-plate composite (SC) walls for accident thermal loading, Nuclear Engineering and Design 295:817-828, https://doi.org/10.1016/j.nucengdes.2015.07.036

[16] Bowerman H., Pryer (1998) Advantages of british steel bi-steel in immersed tunnel construction, Proceedings of the IABSE Colloquim – Tunnel structures. IABSE Reports: volume 78

[17] DOE (2004) Application of Advanced Construction technologies to New Nuclear Power Plants, MPR-2610 Rev2

[18] Sauvageon A. (2016), Instabilités locales de structures en composite acier-béton aux températures élevées, Ph.D. dissertation, Université Paris-Saclay

[19] Sener K.C, Varma A.H (2014) Steel-plate composite walls: Experimental database and design for out-of-plane shear, Journal of Constructional Steel Research 100:197-210, https://doi.org/10.1016/j.jcsr.2014.04.014

[20] Varma A.H., Sener K.C., Zhang K., Coogler K. Malushte S.R (2011), Out-of-plane shear behavior of SC composite structures, Trans. Of the International Assoc. for Struct. Mech. In reactor Tech. Conf., SMiRT-21

[21] McKinley B., Boswell L.F (2002) Behaviour of double skin composite construction, Journal of Constructional Steel Research 58:1347-1359, https://doi.org/10.1016/S0143-974X(02)00015-9

[22] Yan J.B. (2012) Ultimate strength behavior of steel-concrete-steel sandwich beams and shells, Ph.D. dissertation, National University of Singapore

[23] AISC (2015) Specification for safety-related steel structures for nuclear facilities, Supplement n°1, AISC N690-12s1, Chicago, IL, USA

[24] Japan Society of Civil Engineers (JSCE) (2007) Standard specification for concrete structures

[25] Japan Society of Civil Engineers (JSCE) (1992) Design code for steel-concrete sandwich structures

[26] Comité Européen de Normalisation (CEN) (2005) Eurocode 4 – Calcul des structures mixtes acier-béton – Partie 1-1 : Règles générales et règles pour les bâtiments, NF EN 1994-1-1

[27] British standard (1979) Steel, concrete and composite bridges – Part 5: code of practice for design of composite bridges

[28] American concrete institute (ACI) (2008) Building code requirements for structural concrete

[29] Anderson N.S., Meinheit D.S (2007) A review of headed-stud design criteria in the sixth edition of the PCI Design Handbook, PCI Journal

[30] International Federation for Structural Concrete (fib) (2011) Design of anchorages in concrete, Model code bulletin 58

[31] Oduyemi T.O.S, Wright H.D. (1989) An experimental investigation into the behaviour of double-skin sandwich beams, Journal of Constructional Steel Research 14:197-220, https://doi.org/10.1016/0143-974X(89)90073-4

[32] Dogan O., Roberts T.M (2010) Comparing experimental deformations of steel-concrete-steel sandwich beams with full and partial interaction theories, International Journal of the Physical Sciences 5(10):1544-1577, https://doi.org/10.5897/IJPS.9000127

[33] Zhang W., Huang Z., Fu Z., Qian X., Zhou Y., Sui L. (2020) Shear resistance behavior of partially composite Steel-Concrete-Steel sandwich beams considering bond-slip effect, Engineering Structures 210, https://doi.org/10.1016/j.engstruct.2020.110394

[34] Lin Y., Yan J., Wang Y., Fan F., Zou C. (2019) Shear failure mechanisms of SCS sandwich beams considering bond-slip between steel plates and concrete, Engineering Structures 181:458-475 https://doi.org/10.1016/j.engstruct.2018.12.025

[35] Qin F., Kong Q., Li M., Mo Y.L, Song G., Fan F. (2015) Bond slip detection of steel plate and concrete beams using smart aggregates, Smart Materials and Structures 24(11)

[36] Sener K., Varma A.H., Seo J (2016) Experimental and numerical investigation of the shear behavior of steel-plate composite (SC) beams without shear reinforcement, Engineering Structures 127:495-509 https://doi.org/10.1016/j.engstruct.2016.08.053

[37] Yan J.B., Liew J.Y.R., Zhang M.H., Wang J. (2014) Ultimate strength behavior of steel-concrete-steel sandwich composite structures, Part 1: Experimental and analytical study, Steel and Composite Structures, 17(6):907-927 https://doi.org/10.1016/j.oceaneng.2016.03.062

[38] Shanmugam N.E., Kumar G. (2005) Behaviour of double skin composite slabs – an Experimental study, International Journal of Steel Structures 5:431-440

[39] Nguyen N.H, Whittaker A.S (2017) Numerical modelling of steel-plate concrete composite shear walls, Engineering Structures 150:1-11 https://doi.org/10.1016/j.engstruct.2017.06.030

[40] Huang Z., Liew J.Y.R (2015), Nonlinear finite element modelling and parametric study of curved steel-concrete-steel double skin composite panels infilled with ultra-lightweight cement composite, Construction and Building Materials 95:922-938 https://doi.org/10.1016/j.conbuildmat.2015.07.134

[41] Shanmugam N.E., Kumar G., Thevedran V. (2002) Finite element modelling of double skin composite slabs, Finite Elements in Analysis and Design 38:579-599 https://doi.org/10.1016/S0168-874X(01)00093-2

[42] Zhang K., Varma A.H., Malushte S.R., Gallocher S. (2014) Effect of shear connectors on local buckling and composite action in steel concrete composite walls, Nuclear Engineering and Design 269:231-239 https://doi.org/10.1016/j.nucengdes.2013.08.035

[43] Yan J.B. (2015) Finite element analysis on steel-concrete-steel sandwich beams, Materials and Structures 46:1645-1667

[44] Yan J.B., Zhang W. (2017) Numerical analysis on steel-concrete-steel sandwich plates by damage plasticity model: From materials to structures, Construction and Building Materials 149:801-815 https://doi.org/10.1016/j.conbuildmat.2017.05.171

[45] Foundoukos N., Chapman J.C (2008) Finite element analysis of steel-concrete-steel sandwich beams, Journal of Constructional Steel Research 64:947-961 https://doi.org/10.1016/j.jcsr.2007.10.011

[46] Mazars J. (1984) Application de la mécanique de l'endommagement au comportement non linéaire et à la rupture du béton de structure, Ph.D. dissertation, Université Pierre et Marie Curie, Paris 6, France

[47] Hillerborg A., Modéer M., Peterson P.E. (1976) Analysis of crack formation and crack growth in concrete by means of fracture mechanics and finite elements, Cement and Concrete Research, 6:773-792 https://doi.org/10.1016/0008-8846(76)90007-7

[48] van Mier J.G.M. (1984) Strain-softening of concrete under multiaxial loading conditions, Eindhoven

[49] Comité Européen de Normalisation (CEN) (2005) Eurocode 2 – Calcul des structures en béton – Partie 1-1 : Règles générales et règles pour les bâtiments, NF EN 1992-1-1

[50] CEA (2019) Cast3M, available from: http://www.cast3m.cea.fr

[51] SCIENCE (2017). “SC for Industrial, Energy and Nuclear Construction Efficiency”, Research Fund for Coal and Steel (RFCS), RFSR-CT-2013-00017

[52] Burgan B.A., Aggelopoulos E.S. (2017) European design guidance for steel-concrete (SC) structures in nuclear power plant, Trans. Of the International Assoc. for Struct. Mech. In reactor Tech. Conf., SMiRT-24